Journal of Materials Chemistry A

Accepted Manuscript

ROYAL SOCIETY OF CHEMISTRY

www.rsc.org/materialsA

DIPOLAR RELAXATION AND THE IMPEDANCE OF YTTRIA-STABILISED ZIRCONIA CERAMIC ELECTROLYTE

Miguel A. Hernandez and Anthony R. West

Department of Material Science and Engineering, University of Sheffield, Mappin Street, Sheffield, S13JD, UK

Abstract

Equivalent circuit analysis of ac impedance data for yttria-stabilised zirconia ceramics shows evidence for dipole relaxation at intermediate frequencies in addition to long range, oxide ion conduction. Dipoles, or larger clusters, arise from the association between substitutional Y^{3+} ions and oxide ion vacancies. Resistance values for dipole relaxation have similar activation energies to those associated with long range conduction through both bulk and grain boundaries, of approximately 1.1 eV, since both processes involve oxide ion migration.

Introduction

The impedance of most ionically-conducting solid electrolytes can be modelled satisfactorily by a series combination of bulk (i.e. grain) and grain boundary elements together with a third element that represents the impedance of the sample-electrode interface. The bulk ionic conduction in solid electrolytes such as yttria-stabilised zirconia, YSZ, can be regarded as a thermally-generated random walk process involving oxide ions and oxygen vacancies in which an applied bias provides a slight preference, on average, for ions to move in a particular direction, that is given by the polarity of the bias during conductivity measurements.

Ions do not move independently of their surroundings, however [(1)]. First, in a crystalline solid, ions are constrained to migrate between specific sites within the crystal structure and generally follow the pathway that has the lowest activation energy. Second, moving ions are subject to the constraints of the surrounding 'ion atmosphere', a well-known concept in electrochemistry. The ion atmosphere acts as a drag on ion migration which is caused by the departures from local electroneutrality that occur when an ion moves. Reorganisation of the ion atmosphere to restore local electroneutrality is coupled to subsequent hops of the moving ions, leading to the concept (that is difficult to quantify) of many body interactions and their role in conduction mechanisms. Third, a more extreme example of the effect of the ion atmosphere is provided by the occurrence of defect aggregation leading to dipole or cluster formation in which there is an energy of association between oppositely-charged

species. Ions within a cluster may undertake local motions that contribute to dipole reorientation in an applied field, but be unable to take part in long range conduction unless they can overcome the defect association energy and escape from the cluster.

The recognition and measurement of these possible contributions to the overall ionic conductivity of homogeneous materials (and for which, electrical inhomogeneities such as grain boundaries, surface layers and charge depletion effects at sample-electrode interfaces are not significant) is not straightforward. The overall conduction of a material can, of course, be determined readily, either by *dc* measurements if the electrodes are non-blocking to the particular species that is mobile, or by *ac* measurements that are able to relax out sample-electrode contact impedances.

There have been two widely-adopted approaches to evaluate the many-body interactions between a moving ion and its surroundings. Both are based on the observation that the conductivity of a nominally homogeneous material is frequency-dependent over a wide frequency range and cannot be represented by a simple, frequency-independent resistance. The earliest approach, which probably arose from conductivity measurements on glassy materials, was to consider the existence of a distribution of barrier heights for ion migration that was, not unreasonably, associated with a range of available ion sites within the disordered structure of a glass [2,3]. The frequency-dependent conductivity was then attributed to a distribution of 'easy' and 'more difficult' migration steps, depending on the range of barrier heights. Various functions have been proposed to model the distribution of relaxation times that would be necessary.

The second approach to recognition and characterisation of many body interactions arose from Jonscher's Universal Law of Dielectric Response [4]. Properties such as the hopping conductivity of ions and/or electrons have been shown increasingly to follow a very specific power law dependence on frequency. The experimental observation of power law behaviour in many systems, including glasses [5] and single crystal ionic conductors such as Na β-alumina [6], supports the universality of many body interactions; for ionic conductors such as single crystal β-alumina, power law behaviour would be difficult to explain in terms of a realistic distribution of barrier heights to conduction.

Analysis and interpretation of impedance data of ionically-conducting materials, whether single crystals or ceramics, requires the use of equivalent electrical circuits composed of networks of resistors, R and capacitors, C (and sometimes inductors, L). To represent power law impedance behaviour and following the work of Jonscher, a constant phase element, CPE, is incorporated into the equivalent circuits. The admittance, Y^* of a CPE is given by:

$$Y^* = A\omega^n + jB\omega^n \quad (1)$$

where $$B/A = \tan(n\pi/2) \quad (2)$$

A characteristic feature of a CPE is that it gives a power law dependence on frequency of both the resistive and capacitive components of the admittance. The CPE is usually added in parallel with (i) a resistance, R, that corresponds to the limiting low frequency, or *dc*, resistance of the sample and (ii) a capacitance, C, that corresponds to the limiting high frequency permittivity, often referred to as ε_∞, to give the equivalent circuit shown in Fig 1(a). Such an element, (R_1-C_1-CPE_1), represents accurately the typical bulk impedance response of numerous ionic and electronic hopping conductors at high frequencies [7-13]. Recognition of the usefulness and indeed, validity, of CPEs allows accurate modelling of combined bulk conductivity and permittivity data over wide ranges of frequency. This is because the circuit element in Fig 1(a) incorporates both the 'ideal', frequency-independent R and C parameters and the power law components of the CPE.

In addition to hopping ionic conduction which is characterised by both frequency-dependent *ac* conductivities at high frequencies and limiting, frequency-independent *dc* conductivities at low frequencies, it may be necessary to include in equivalent circuit representations, the possibility of local ionic motions that are unable to contribute to long range conduction . This is exemplified by polar dielectrics which are both electrical insulators at low frequencies since the mobile component of the polar dielectric is trapped within the environment of the dipole, but are also able to exhibit local atomic motions such as dipole reorientation. The equivalent circuit representation of such dipolar reorientation is, in its simplest form, given by a series RC element, Fig 1(c), in which R represents the resistance associated with the local hops and C is the effective amount of charge stored by the reoriented dipoles. The series capacitance is a block to any long range ionic conduction.

The methodology used to analyse and interpret conductivity and capacitance data depends traditionally on whether the materials of interest are primarily conductors or dielectrics. For conducting materials, equivalent circuit representation is now commonly-used, following the work of Bauerle [14], in which series combinations of parallel RC (and CPE) elements represent grain, grain boundary and sample-electrode interface impedances. The data are often fitted to the appropriate equivalent circuit and values for the component R, C and CPE parameters extracted; it is, however, less common to consider dielectric relaxation processes as part of an overall impedance response.

For dielectric materials, by contrast, equivalent circuit analysis is not usually used; instead, data are presented as tan δ against either frequency for fixed temperature measurements or

temperature for fixed frequency measurements; peaks are identified and correlated with relaxation processes in the sample; any *dc* conduction appears as a background loss.

The family of stabilised zirconias represented by YSZ is of much interest for solid oxide cell applications due to their high levels of oxide ion conductivity at high temperatures [15,16]. Many impedance studies on YSZ and related materials, both single crystals and ceramics, have been reported; some key examples are as follows. Single crystals of YSZ10 (containing 10 mol% Y_2O_3) showed a single, slightly broadened arc in impedance complex plane plots. The dispersion in electrical properties was assigned to charge carrier relaxation and fitted to an approximately Gaussian distribution of relaxation times [17]. Single crystals of YSZ9 showed dispersions in permittivity, from which tan δ peaks were extracted and attributed to defect associates involving substitutional Y and oxygen vacancies [18].

The impedance of YSZ ceramics containing 3-12 mol% Y_2O_3 showed three components attributed to grains, grain boundaries and electrode contacts; the high frequency bulk conductivity data showed power law dispersions, from which defect association energies were obtained and found to increase with Y content to a maximum value of 0.19 eV [19]. The conditions used to sinter YSZ8 ceramics had a significant effect on both the resulting microstructures and the associated impedance data; a complex interplay between grain and grain boundary impedances was found to be responsible for the dependence of total conductivity on sintering temperature, which passed through a maximum for samples sintered at ~1350 ^{o}C [20]. The effect of porosity was assessed by comparing the impedance of samples sintered with and without a ceramic filler; in the first case, an extra, intermediate frequency arc was observed and attributed to pores acting as a blocker of oxide ion conduction [21].

There are, therefore, numerous evidences and suggestions in the literature for the effect of defect association on the electrical properties of YSZ. Defect association is also thought to be responsible for commonly-observed curvature of conductivity Arrhenius plots, in which the higher activation energy at lower temperatures contains a contribution from the activation energy for defect dissociation; curvature is not always observed however, as in the case of CaO-stabilised zirconia single crystals [22]. Similarly, decreases in conductivity on annealing samples of various doped zirconia compositions at intermediate temperatures, known as ageing phenomena, are attributed to the trapping of mobile oxygen vacancies in defect clusters. Nevertheless, as far as we are aware, direct, unambiguous evidence for the contribution of dipole relaxation to overall impedance data has not been obtained. This is probably because, as shown by our results, dipole relaxation is not responsible for a separate arc in the impedance response but is incorporated into the bulk arc; its presence

becomes apparent only on detailed circuit fitting. In this paper, we present an equivalent circuit analysis of impedance data and, from the need to include an extra component in order to model satisfactorily the impedance response, present evidence for the contribution of dipole relaxation.

Experimental

YSZ powder (8 mol% Y_2O_3, 92 %ZrO_2, TOSOH zirconia powder TZ-8YS, crystallite size 540 Å, specific surface area 6.0 $m^2 g^{-1}$) was used as-received. Pellets were pressed uniaxially at 1.5 MPa, placed on Pt foil and sintered at temperatures in the range 1350–1600 ^oC for 2 h using heating and cooling rates of 5 ^oC /min. Pellet densities were calculated from their mass and dimensions and were in the range 85-92 %. Electrodes were made from three materials, Pt paste, Au paste and sputtered Au. For the paste electrodes, samples were heated at 900 ^oC (Pt) and 800 ^oC (Au) for 2 h to decompose and harden the paste. Samples with electrodes attached were placed in conductivity jigs, attached to Pt leads and located inside a horizontal tube furnace. Impedance measurements were made over the temperature range 200 to 700 ^oC and frequency range 10^{-1} to 10^7 Hz using a Solartron Modulab Xm and 10^2 to 10^7 Hz using an Agilent E4980A impedance analyser; sometimes, the low frequency data points showed scatter and in that case, were excluded from detailed circuit fitting analysis. Data were routinely collected in air but the atmosphere for some measurements was changed to flowing O_2 or N_2. Data were analysed using Zview2 software.

Results

A collection of typical impedance data sets at three temperatures is shown in Fig 2. All data sets showed three similar features, although not all features were seen at every temperature due to frequency limitations of the measuring equipment. A first assignment of the three features was made based on the magnitudes of the associated capacitances [(23)]. Thus, the high frequency arc was attributed to the bulk response, the intermediate frequency arc to a grain boundary impedance and the low frequency inclined spike to a sample-electrode contact impedance.

If these assignments are correct, an equivalent circuit similar to those shown in Figs 1(b,d) should provide a reasonable fit to the data. Element R_1-C_1-CPE_1 should fit the high frequency arc and departures from the ideality of an undistorted semicircle should be taken care of by the element CPE_1. Element R_2C_2 should fit the intermediate frequency arc, although a second CPE in parallel with R_2C_2 may be needed to obtain a good fit. Element CPE_3 should fit the low frequency spike, provided it is linear.

Attempts to fit the experimental data to circuit Fig 1(d) were unsuccessful, as shown by the poor quality of the agreement at intermediate frequencies between experimental and fitted data in Fig 3(b). It is clear, therefore, that a circuit representing bulk and grain boundary impedances, in series, does not adequately represent the impedance of the YSZ ceramics studied here, although it is an appropriate circuit for many other ionically- and electronically-conducting materials.

We therefore consider the possibility that dipoles or defect clusters associated with oppositely-charged species such as Y'_{Zr} and $V_O^{\cdot\cdot}$, are likely to be present in the YSZ crystal structure, may be able to change their orientation by means of oxygen vacancy hops around the Y dopant and may therefore contribute to the measured impedance data. These localised hops are distinct from those of 'free' oxygen vacancies which are able to take part in long range conduction. To represent this, it is necessary to add a series R-C element, Fig 1(c), to the equivalent circuit for the YSZ ceramics and for this to be in parallel with the R_1 element that represents long range conduction. *This element cannot be in series with R_1 since the series capacitance would prevent long range conduction from occurring, in contradiction to the observed high levels of dc ionic conductivity in YSZ.* The circuit shown in Fig 1(e) now contains both conducting and dipolar impedance components. Fits of experimental data to this circuit at the same three temperatures are shown in Fig 3(a); the agreement is good.

The presentation of results in the impedance complex plane, Z'' vs Z', highlights the most resistive components of impedance data but suffers from the disadvantage that, when plotted on the usual linear scales, low resistance impedances are effectively hidden from view by much larger impedances. In order to assess the fit quality over the entire frequency range, it is necessary to use one of two possible alternative data presentation strategies; our preference is to use of logarithmic scales since this gives equal weighting to all data points over the entire frequency range, as well as a visual estimation of fit quality. An example is shown in Fig 4 in which the same data are plotted as either log C' or log Y' vs log ω. In both cases, excellent agreement is seen over the entire frequency range. The alternative approach is to plot, in addition to the experimental and fitted data, the residuals between experimental and fitted data as a function of frequency.

From the fits, values of the various R, C and CPE parameters were extracted and are summarised as a function of temperature in Fig 5 and Tables 1 and 2. Capacitance data were found to be independent of temperature, within errors. Data are given for samples sintered at temperatures in the range 1350 to 1600 ^{o}C and using three different electrode materials.

Discussion

The impedance data of YSZ ceramics sintered at temperatures in the range 1350–1600 ^{o}C cannot be modelled accurately using the conventional circuit for ionic conductors that consists of a series combination of bulk and grain boundary impedances. In particular, the higher frequency data that represent the bulk response show significant departure from the response of a single parallel R-C-CPE element; an additional component in the equivalent circuit is required to fully model the bulk response. Good fits are obtained by the inclusion of a series element, R_d-C_d which effectively adds a dielectric, but locally conductive, component in parallel with the long range conductivity represented by the bulk element, R_1-C_1-CPE_1. The extra series component is attributed to the reorientation of dipoles or clusters that, in their simplest form, may be represented by Y'_{Zr}– $V_o^{\cdot\cdot}$, in which positively-charged oxygen vacancies are trapped by, but can hop around, the negatively-charged, substitutional Y^{3+} ions.

From visual inspection of impedance complex plane plots, the possible presence of a dielectric element in the equivalent circuit is not immediately apparent since it does not generate a separate arc or semicircle. For this reason, the standard procedure and a logical first step in data analysis is to assign the two observed arcs, such as those in the Fig 2 datasets, to a series combination of bulk and grain boundary impedances. It is only when circuit fitting is attempted using standard circuits, such as shown in Fig 1(b) or (d), that the need to include an extra element becomes apparent. One possibility would be to add an additional, low capacitance element in series but, given that the bulk and grain boundary responses have already been included, it may be difficult to find a sample-related origin for such a third component. The need for the additional component was apparent for a range of YSZ samples, sintered at different temperatures and with different electrodes, and was therefore an intrinsic effect in the samples and not, for instance associated with surface phenomena or electrode-sample contacts. By contrast, the inclusion of the additional, parallel dielectric element gives a good fit to experimental data, has a logical explanation in terms of the defect structure of the YSZ ceramics; it forms the basis of the discussion that follows.

The activation energy for dipole reorientation, R_d^{-1} is in the range 1.00 – 1.17 eV, Table 1 which is comparable to that for both long range bulk conduction, R_1^{-1}, 1.00 – 1.08 eV, and grain boundary conduction R_{gb}^{-1}, 1.02 – 1.15 eV. This indicates that a similar hopping process, involving oxide ion vacancies, is involved in all three resistances. In particular, the

hopping involved in dipole reorientation is essentially the same process as that involved in long range conduction but is constrained capacitively to the immediate environment of the Y^{3+} ions.

The magnitudes of the three resistances depended somewhat on the sample sintering temperature, Fig 5, but were independent of the electrode material and preparation. In particular, sintering at 1450 ^{o}C gave the highest values for the bulk conductivity, R_1^{-1} and smallest values for the dipolar conductivity, R_d^{-1} which implies that fewer oxygen vacancies were trapped in the dipoles at 1450 ^{o}C. A similar maximum in the bulk conductivity of film samples sintered at 1450 ^{o}C has been reported [24]; this, and a maximum in the overall conductivity of samples sintered at 1350 ^{o}C [20], were attributed to microstructural differences in samples sintered at different temperatures.

The effect of porosity on the impedance response of YSZ ceramics has been considered [21]; a model for constriction resistances associated with porous Li^+ ion conducting ceramics has been proposed [25] which has the characteristic feature of a similar activation energy for bulk and constriction resistances provided the same material and conduction mechanism is responsible for the two impedances. The present results, tables 1 and 2, show a grain boundary resistance, R_{gb}, with a similar activation energy to that of R_1 that may also, therefore, be constrictive in nature. Although constriction resistances involve partial blocking by the pores and air gaps, they are conventional impedances in series with the bulk impedance, rather than entirely blocking, dielectric impedances in parallel with the main conduction pathways. We cannot assign the dielectric element, R_d-C_d, to a sample porosity effect, therefore.

The present results indicate that, as well as the complexity of the grain and grain boundary microstructure and associated electrical properties of YSZ ceramics which, from the literature, are still not fully understood, the degree of defect association also has a significant influence on the bulk, long range conductivity of YSZ ceramics. Further work is required to understand the link between sample processing conditions and dipole formation and how such defect association can be minimised.

The equivalent circuit used to model and fit the data successfully, Fig 1(e), contains a CPE that effectively, introduces variable resistors and capacitors which are able to account for departures from the ideality that would be expected for a circuit composed only of frequency-independent R,C elements. At the simplest level, a CPE is an empirical circuit fitting parameter, but some insight into its possible significance is given by the parameter *n* which takes values in the range $0 \leq n \leq 1$. For $n = 0$, the CPE is purely resistive; for $n = 1$ it is purely capacitive; for intermediate values, it represents the contribution of resistive and

capacitive components to the associated *ac* impedance. It has been shown by Almond *et al* that distributed networks of R,C elements are able to represent the electrical properties of composite materials composed of interpenetrating networks of conductive and dielectric components [26,27] and that the *n* parameter derived from the power law dependence of conductivity and capacitance on frequency is related directly to the number of R and C components in the network. Qualitatively, therefore, the capacitive components of the network, and the range of relaxation times associated with the many possible R-C pairings within the network, may be understood in terms of the many body nature of conduction processes and the drag on long range conduction, at low frequencies, associated with the ion atmosphere.

The equivalent circuit shown in Fig 1(e) contains 10 variables (including 2 variables in the CPE). Great care was required to establish that this was the most appropriate circuit since undoubtedly, various other 10-parameter circuit combinations could also be used to fit experimental data. The importance of using the correct circuit is that the equations used to extract values of R and C components depend implicitly on the circuit used. Use of the correct circuit is therefore essential in order to attribute physical significance to the parameters and their values. Unfortunately, it can be very easy to fit data to more than one possible circuit that has 10 variables, but much more difficult to ascertain whether the chosen circuit is the best possible representation. Additional help is therefore required and, as discussed above, the second step in circuit analysis is to consider the physical characteristics of the sample and make an assignment of the various circuit elements to electrical features of the sample.

The strategy adopted here was, as shown previously[7], to commence with impedance data recorded at the lowest temperatures and for which the bulk response only was observed, fit these data to the bulk element shown in Fig 1(a) and then gradually incorporate more elements to fit the lower frequency components seen at higher temperatures. With increasing temperature, less of the high frequency component was seen in the impedance results and the parameters C_1 and *n* were fixed at the values obtained at lower temperatures, thereby reducing the number of variables in the refinements.

A characteristic of CPE elements is that they may contribute to the overall impedance over very wide ranges of frequency. For the bulk element shown in Fig 1(a), Y' data at high frequency are dominated by the CPE and conversely, C' data at low frequency are dominated by the CPE. We did not include a second CPE in the element that represents the grain boundary impedance in Fig 1(e), partly because a satisfactory fit was obtained without adding a second CPE but also because, it can be difficult to obtain a unique solution in a

refinement which contains two (or more) CPEs, both of which are frequency-dependent. For similar reasons, we did not include a CPE in the dipolar component of the circuit, Fig 1(c).

Data for the temperature dependence of the A component of the CPE are shown in Fig 5 and Table 1. We observe an approximate correlation between n_1 and the activation energies of R_1^{-1} and A_1, given by:

$$E_{A1} = (1 - n)\, E_{R1}^{-1} \qquad (3)$$

Thus, typical activation energies for R_1^{-1} and A_1 are ~1.0 and 0.3 eV, respectively with an n value of ~ 0.7. Such a correlation was first noticed in conductivity data of the Na^+ ion conductor β-alumina[28] and indicates that the temperature-dependence of the CPE is due to that part of the CPE which is resistive.

Conclusions

It is widely believed that defect association occurs in YSZ ceramics and has a major influence on the dependence of conductivity on temperature and dopant (divalent and other trivalent ions, as well as Y^{3+}) concentration. Nevertheless, to the best of our knowledge, direct information on dipole reorientation processes, and their contribution to frequency-dependent conductivity, has been difficult to obtain.

Analysis and interpretation of impedance data requires fitting to an equivalent circuit; values obtained for the various R and C components depend critically on the equation of the equivalent circuit and it is essential to establish which circuit best models a given impedance data set. A major complication in circuit fitting is that data rarely fit circuits composed of ideal, frequency-independent, single-valued, R and C components. In order to account for such departures from ideality, constant phase elements are widely added to the equivalent circuits and generally provide a good fit to experimental data, especially for materials in which the impedance is best represented by a series combination of grain, grain boundary and electrode contact impedances.

The data for the YSZ samples studied here cannot be fitted to such a circuit of three, series-connected impedances. We therefore introduce an additional element, in parallel with the element that represents bulk ionic conduction, to model a local conduction process associated with reorienting dipoles. Good quality fits to the impedance data are then obtained, enabling values for the various circuit components to be extracted, including their variation with temperature. The circuit therefore has three sample-dependent components

that represent grain (or bulk) conduction, grain boundary conduction and dipole relaxation, together with sample-electrode contact impedances;

the dipole relaxation component does not give a separate arc in the impedance complex plane but instead, is combined with the bulk conduction component.

We believe that this is the first time that direct evidence has been obtained for such dipole reorientation processes at the same time as long range conduction. Interestingly, the activation energy for dipole reorientation is comparable to that for long range conduction, which is not surprising since ion hopping involving oxygen vacancies, is essentially the same in both processes.

Acknowledgements

We thank the Erasmus programme for financial support (MAH)

References

1. A.D. Le Claire, in Physical chemistry, an advanced treatise, Chapter 5, Eds H. Eyring, D. Henderson and W. Jost, Academic Press **10** (1970) 261

2. C.A. Angell, Chem. Rev., **90** (1990) 523

3. J.C. Dyre, J. Appl. Phys., **64** (1988) 2456

4. A.K. Jonscher, Nature, **267** (1977) 673

5. H. Jain and S. Krishnaswami, Solid State Ionics, **105** (1998) 129

6. R.J. Grant, I.M. Hodge, M.D. Ingram and A.R. West, Nature, **266** (1977) 42

7. E.J. Abram, D.C. Sinclair and A.R. West, J. Electroceram., **10** (2003) 165

8. N. Maso, X.Y. Yue, T. Goto and A.R. West, J. Appl. Phys., **109** (2011) 024107

9. A. Perejon, N. Maso, A.R. West, P.E. Sanchez-Jimenez, R. Poyato, J.M. Criado and L.A. Perez-Maqueda, J. Amer. Ceram. Soc., (2013) 1

10. P.G. Bruce, A.R. West and D.P. Almond, Solid State Ionics, **7** (1982) 57

11. P.G. Bruce and A.R. West, J. Electrochem. Soc., **130** (1983) 662

12. D.P. Almond, G.K. Duncan and A.R. West, J. Non-cryst. Solids, **74** (1985) 285

13. R.A.M. Osman and A.R. West, J. Appl. Phys., **109** (2011) 074106

14. J.E. Bauerle, J. Phys. Chem. Solids, **30** (1969) 2657

15. S.P.S. Badwal, Mat. Sci. Tech., A Comprehensive Treatment **11** (1996) 567

16. A.J. Jacobson, Chem. Mater., **22** (2010) 660

17. S. Kazlauskas et al, Solid State Ionics, **231** (2013) 37

18. H. Yamamura et al, J. Ceram Soc. Japan, **115** (2007) 546

19. J. Luo et al, J. Am. Ceram. Soc.,**83** (2000) 1703

20. X.J. Chen et al, Mat. Sci. Eng. A, **335** (2002) 246

21. R. Muccillo, J. Mater. Res., **24** (2009) 1780

22. A. Orliukas, P. Bohac, K. Sasaki and L. Gauckler, J. Eur. Ceram. Soc., **12** (1993) 87

23. J.T.S. Irvine, D.C. Sinclair and A.R. West, Adv. Mater., **2** (1990) 132

24. T. Talebi, M. Haji and B. Raissi, Int. J. Hydrogen Energy, **35** (2010) 9420

25. P.G. Bruce and A.R. West, J. Electrochem. Soc., **130** (1983) 662

26. D.P. Almond, C.R. Bowen and D.A.S. Rees, J. Phys. D: Appl. Phys., **39** (2006) 1295

27. D.P. Almond and B. Vainas, J. Phys.: Condens. Matter, **11** (1999) 9081

28. D.P. Almond, A.R. West and R.J. Grant, Solid State Comm., **44** (1982) 1377

Figure Captions

1. Equivalent circuits for modelling impedance data.

2. Typical impedance data for YSZ ceramics at three temperatures.

3. (a) Equivalent circuit and fits to impedance data, (b) poor quality fits to an equivalent circuit lacking a dielectric component.

4. Fits of the equivalent circuit to C' and Y' presentations of data on logarithmic scales.

5. Arrhenius plots of the various resistance parameters

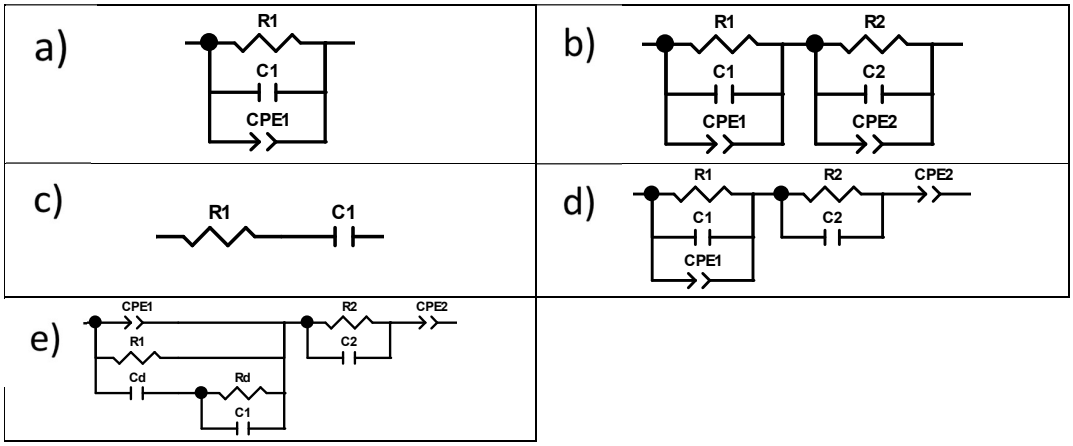

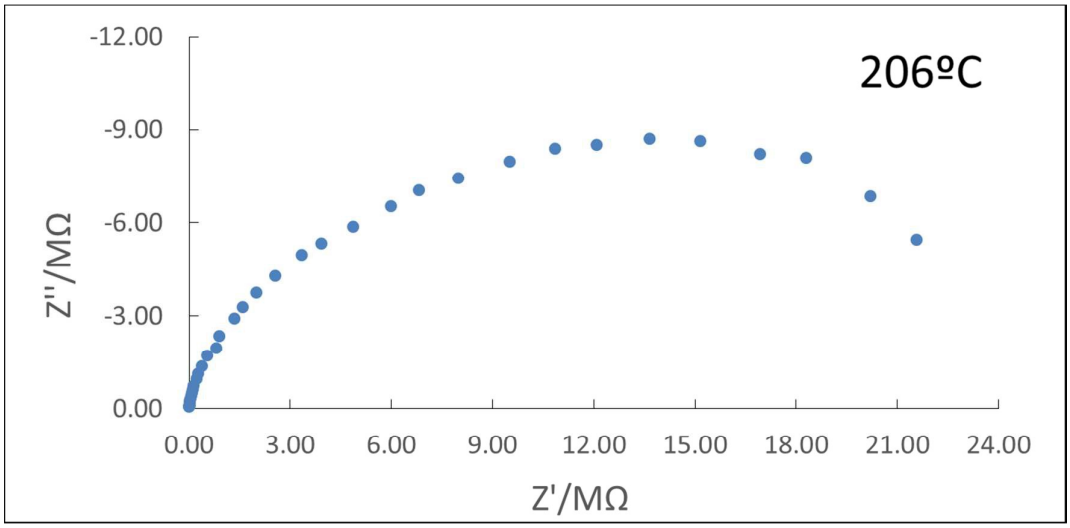

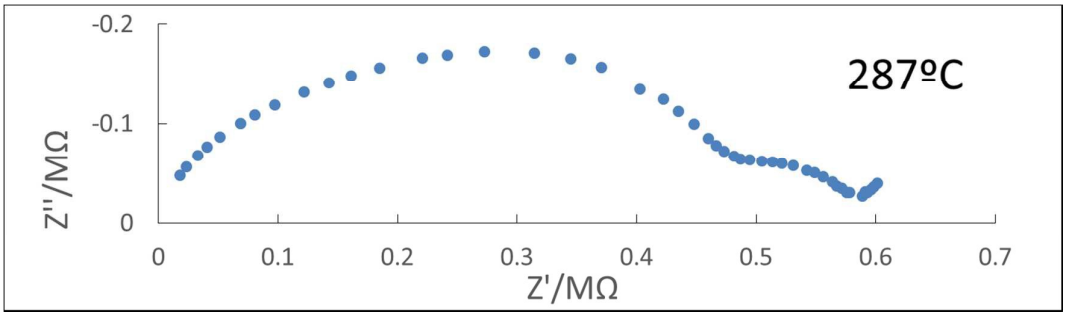

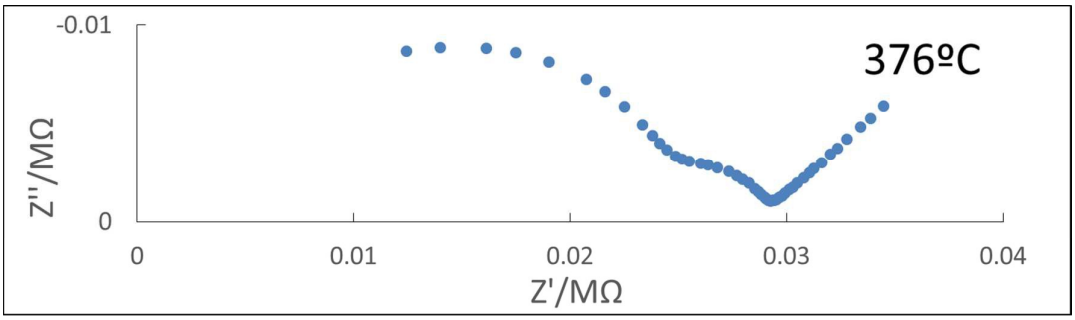

a)

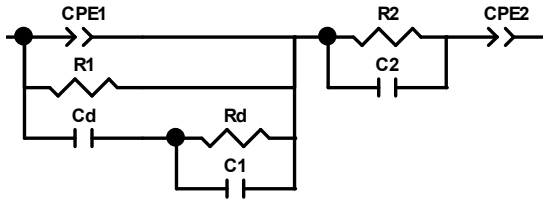

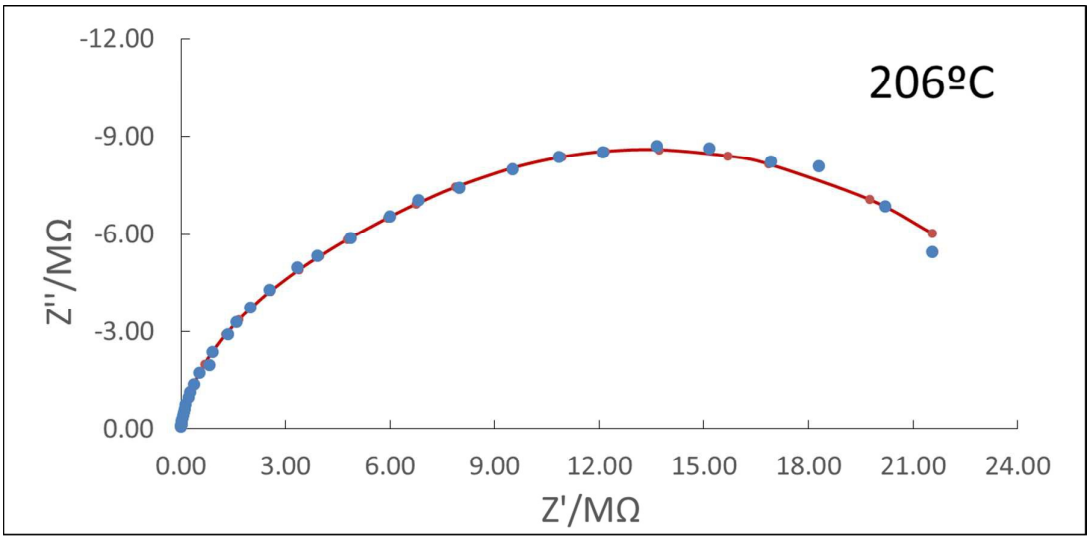

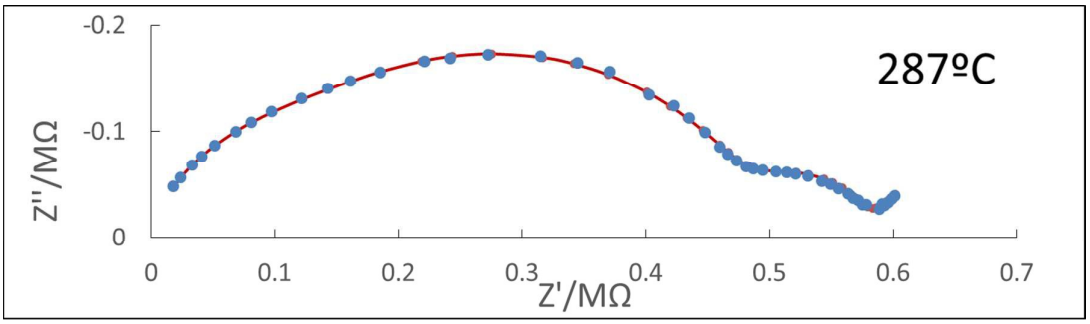

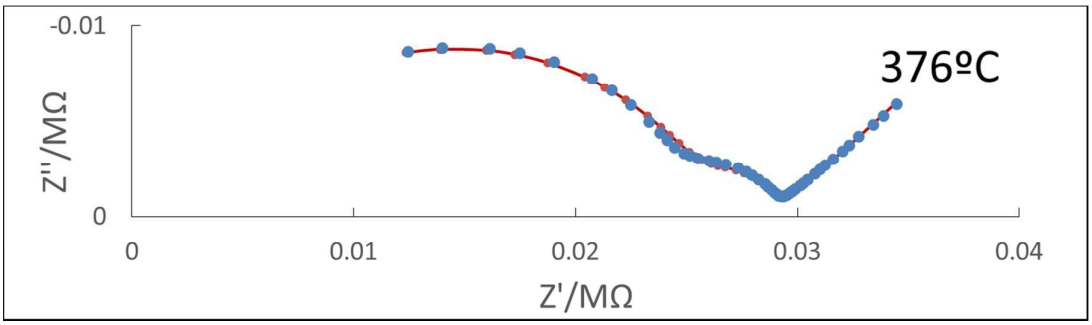

b)

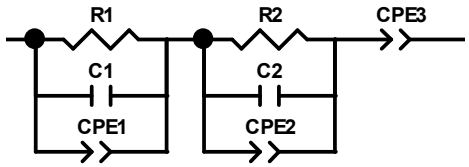

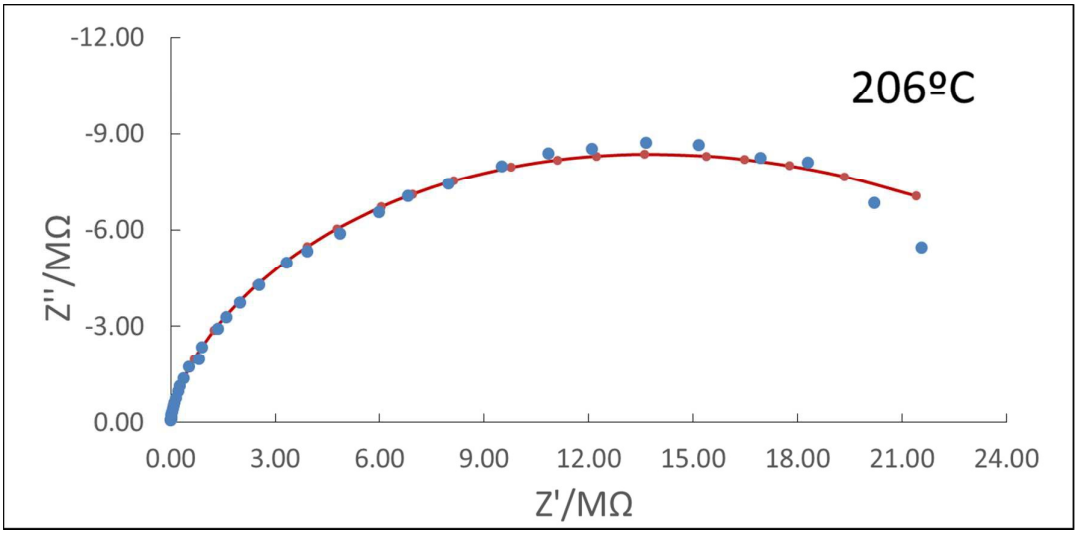

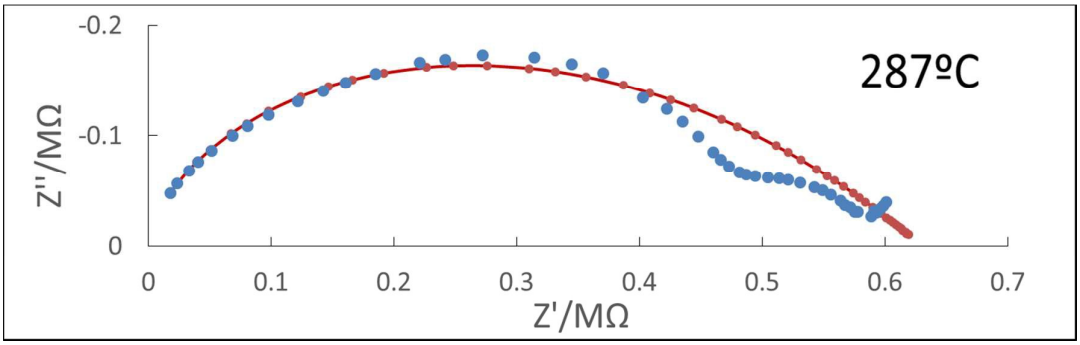

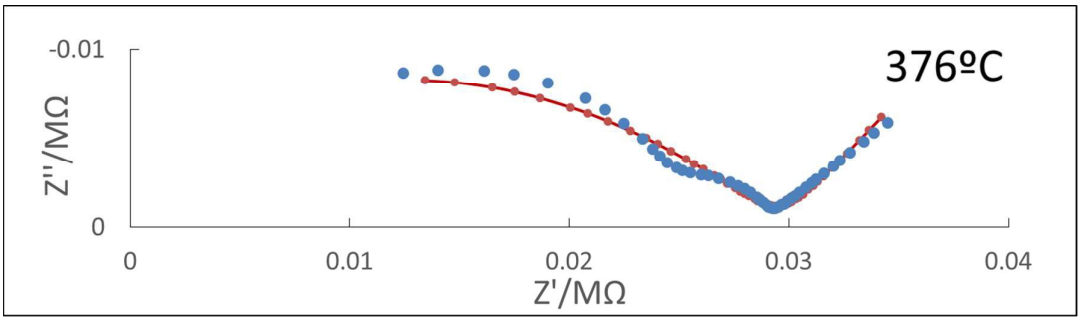

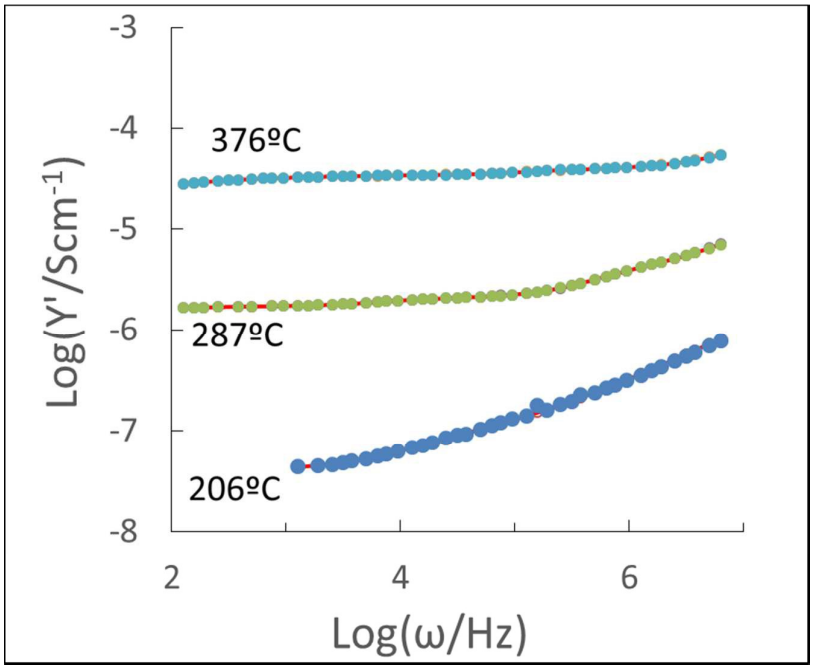

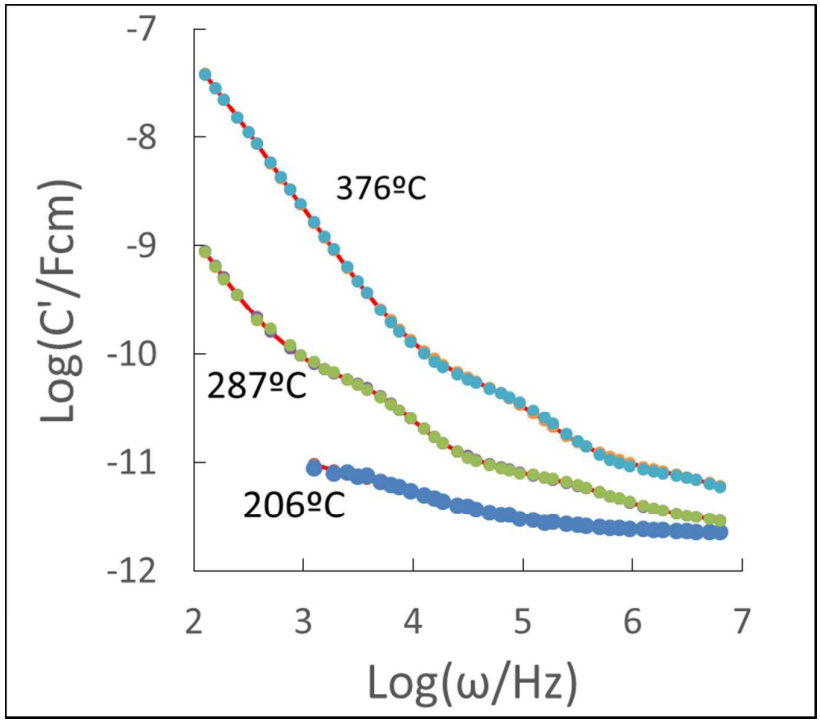

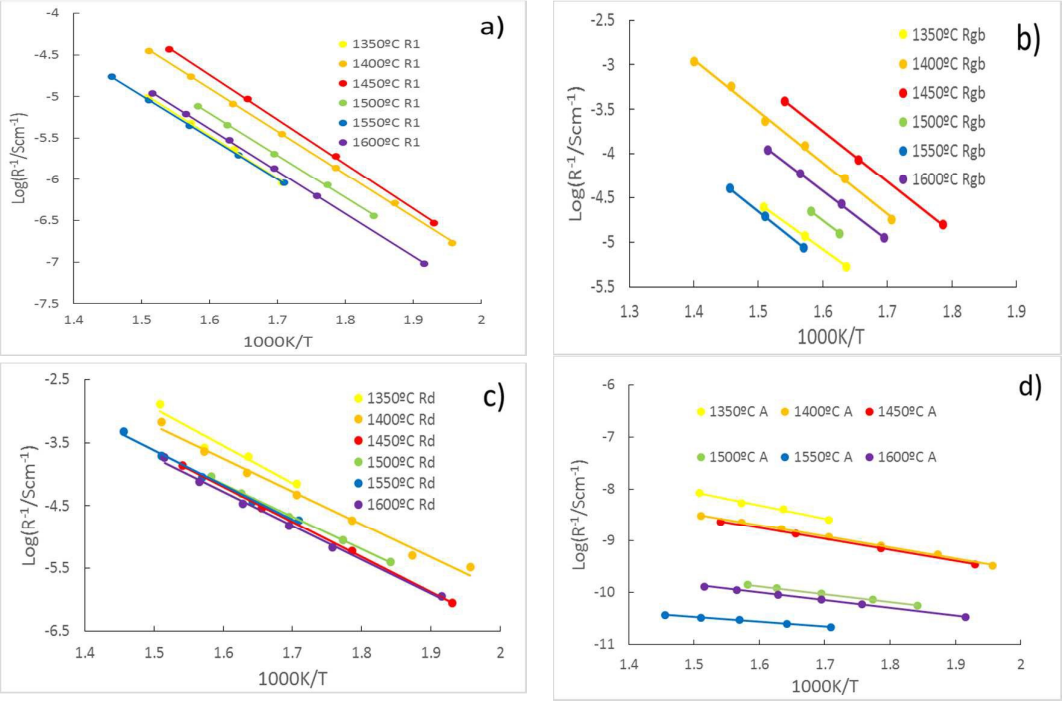

Table.1. Activation energies, capacitances and CPE parameters for different sintering temperatures, Pt electrodes.

T(ºC)	1350	1400	1450	1500	1550	1600
E.R_d (eV)	1.17(4)	1.03(9)	1.11(1)	1.03(1)	1.09(7)	1.08(1)
E. R_1(eV)	1.03(2)	1.02(4)	1.06(8)	1.00(9)	1.00(1)	1.02(3)
E.A(eV)	0.50(6)	0.42(9)	0.42(6)	0.30(6)	0.18(1)	0.29(3)
E.R_{gb} (eV)	1.02(9)	1.15(4)	1.13(4)	1.11(6)	1.15(3)	1.09(4)
C_d(pF)	3.35	3.21	3.42	1.51	2.83	1.79
C_1(pF)	0.24	0.24	5.17	5.21	0.11	3.90
n	0.39	0.56	0.58	0.69	0.79	0.71
C_{gb}(nF)	0.44	3.39	4.61	1.30	0.99	2.04

Table.2. Activation energies, capacitances and CPE parameters for different sintering temperatures, Au electrodes.

	Au(P)1450ºC	Au(P)1600ºC	Au(SC)1450ºC	Au(SC)1600ºC
E.$\mathbf{R}_d$ (eV)	1.11(5)	1.00(3)	1.08(6)	1.03(8)
E. R_1(eV)	1.08(6)	1.04(6)	1.06(3)	1.00(6)
E.A(eV)	0.36(4)	0.34(2)	0.39(8)	0.28(1)6
E.R_{gb} (eV)	1.14(1)		1.12(3)	
C_d(pF)	2.97	2.34	2.85	2.92
C_1(pF)	8.03	3.78	0.11	2.01
n	0.693	0.676	0.607	0.7
C_{gb}(nF)	5.74		6.8	